Chapter 2
Surface Integrity of LY2 Al Alloy Subjected to Laser Shock Processing

Abstract This chapter presents a comprehensive literature review of the physical and mechanical mechanisms of LSP on metallic materials, which have been investigated in the past 30 years. In particular, more attentions have been focused on the effects of LSP on mechanical properties of LY2 Al alloys are also highlighted.

2.1 Introduction

Since laser shock processing (LSP) was invented in the early 1960s, lots of studies mainly focused on the physics process, the physical mechanisms, the plasma to achieve high pulse pressures [1] and the development of mathematics models to characterize LSP processes [2].

Since 1990, many researchers [3–8] have further developed and enriched this technique by investigating the effects of laser spot shape, characteristics of shock waves and their propagation on the induced mechanical properties. More attention on laser shock processing was paid to some important processing parameters related to LSP conditions, such as laser processing parameter, confined layer and absorbing coatings, which can significantly affect the mechanical properties of the alloys and metallic materials.

This chapter presents laser systems of LSP, particularly addressing its physical mechanisms and effect on the surface integrity of Al alloy. Emphasis is put on LSP processing parameters including laser power density, laser spot, as well as LSP impact number and the coverage ratio of LSP impacts on the nano-hardness, residual stress and surface topography of LY2 Al alloy.

Y. Zhang et al., *Laser Shock Processing of FCC Metals*,
Springer Series in Materials Science 179, DOI: 10.1007/978-3-642-35674-2_2,

2.2 Laser Systems for Laser Shock Processing

In order to meet the LSP process requirements, laser requires an average power level from several hundred watts to kilowatts, a pulse energy with several ten Joule and a pulse duration with 8–30 ns. Repetition rate of the laser system and a reasonable laser wavelength are also important parameters for LSP to achieve effective strengthening effect for alloys and metal components.

Neodymium-doped glass (Nd: glass) laser was firstly developed in 1974 at Battelle–Columbus Laboratories Ohio. The repetition rate of this laser with wavelength of 45 m long and with pulse power of 500 J was extremely low, and one cycle can be obtained every 8 min. In 1992, Battelle–Columbus Laboratories invented a $\sim 1.2 \times 1.8$ m Nd: glass laser system with a repetition rate of 1 Hz and a pulse energy of around 100 J based on the above-mentioned technology [9].

Lawrence Livermore National Laboratory (LLNL) has developed high-power Nd: glass laser systems for LSP applications over the past 30 years [10]. These laser systems can deliver average pulse energy of 25–100 J and repetition rates of up to 10 Hz.

The common laser system used for laser shock processing is a high-energy, the wavelength of pulsed Nd: glass laser system is about 1,054 nm high. Suitable laser peening systems can produce short laser pulses, from about 8–30 ns in pulse duration, where the beam energy is in the range of 10–50 J. Although laser systems with lower energy, small spot size or ultra-short pulse durations have been considered, these systems typically do not provide enough power to create the desired effect.

Either circular or square-shaped laser spots can be used depending on the configuration of the laser system and optical components. The laser spot size may be adjusted with lenses, but it is typically an area in the range of 3–28 mm^2 that is applied to the part. The LSP parameters are typically selected to achieve a power density or laser irradiance of 5–10 GW cm^{-2}. A two-beam laser system may be used advantageously to impact the opposite sides of thin parts, such as the edges of turbine engine airfoils. Laser shock processing one side of a thin blade completely and then the opposite side can result in an excessive distortion. However, this can be avoided by using an alternating scheme in which a laser beam is applied first to one side of the blade and then a second beam is applied to the opposite side. Figure 2.1 shows a two-beam laser system that operates at 50 J per beam.

In the early 1990s, laser systems were not commercially available with the power or laser repetition rate to make laser peening practical. Typically, laser fluence in the range of 100–200 J cm^{-2} is required to create the desired effect in most materials. Early laboratory-based systems had a repetition rate of only one pulse every 8 min. As a consequence, the coverage rate for laser-peening parts was far too slow. The first generation of laser-peening systems was designed with a series of laser amplification stages (all using flash lamps) and an advanced electronic control system. This boosted the laser beam from an oscillator to produce two beams having beam energy up to 50 J per beam and a laser repetition rate of one pulse every 8 s (0.125 Hz).

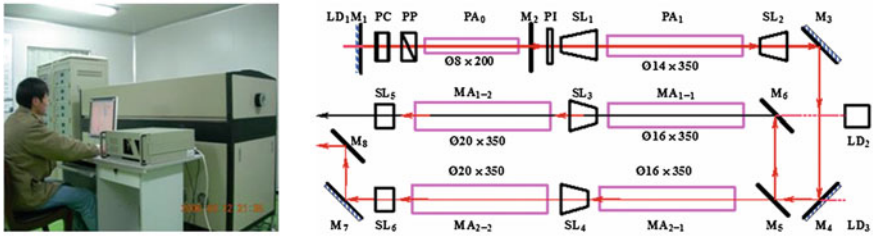

Fig. 2.1 High-power and repetition-rate Nd: glass pulse laser shock equipment manufactured by Jiangsu University and the light-road layout of laser head. *LD1* ~ *LD3* Semiconductor laser; *M1* 0° mirror; *M2* output mirror, *M3, M4, M6* ~ *M8* 45° mirror; *M5* 45° half-mirror; *PC* KD*P pockels cell; *PP* polarizer; *PI* isolator; *SL1* ~ *SL6* laser bean expander; *PAm, MAm-n* Nd: glass rod

To create the first practical industrial LSP systems, the life and reliability of the laser system components had to increase. The electronics for the pulse-forming networks were redesigned to produce a laser repetition rate of one pulse every 4 s (0.25 Hz) and assembled into modules for easy replacement in case of failure. The materials used for the flash lamp reflectors and the procedures used to produce the laser rods were optimized to boost efficiency and to extend component life. Under the support of the US Air Force ManTech program, LSP Technologies refined LSP technology by building a system with industrially hardened environmental controls and many quick-change features for parts requiring repair or routine maintenance, and boosting the laser repetition rate to one pulse every 0.8 s (1.25 Hz) [11].

Each increase in repetition rate required further improvements to the optical system components to avoid damage during operation. Even higher laser repetition rates for LSP systems are possible (3–5 Hz), even at lower energy levels and using smaller spots. However, laser repetition rate cannot the complete answer to boosting the coverage rate. One must also consider the requirements for applying and replenishing the opaque confined layer and handling the parts. According to these requirements and the laser system, practical LSP coverage rates can be typically 10–20 cm^2 min^{-1}.

The latest laser-peening systems incorporate improved diagnostics to monitor and control the beam's spatial profile (to assess the energy distribution within the laser spot) and temporal profile (to measure the uniformity of the laser pulse timing). These systems also include electronic features for optimizing the shape of the laser pulse to create a uniform shock wave at the surface of the part. This provides a more uniform compressive residual stress distribution in the part being treated.

2.3 Generation of Laser Shock Wave

Shock waves can be generated when a laser pulse with high enough power density hits a metal surface. In this way, Q-switched lasers can generate GW laser beams of 1–100 + J pulses less than 100 ns in the action time.

The shock wave propagating into the metal can cause the plastic deformation, which results in the compressive residual stresses in the surface layer of alloys and metallic materials. The generation and physical mechanisms of laser shock wave has been investigated intensively [12–17]. In early published experiments [18, 19], the treated target was in a vacuum and the laser produced a plasma that expanded freely. The resulting peak pressures of laser induced shock wave ranged from 1 up to 10 GPa when the incident laser power density varied from about $0.1–10^6$ GW/cm^2. The time duration of the shock wave pressure pulse was roughly 3–4 times as long as the laser pulse duration in air, but the time duration was only equal to the laser pulse duration in the vacuum because of the rapid adiabatic cooling of the laser generated plasma [20].

The transparent confined layer has been used to increase the intensity of laser shock wave propagating into the metal by up to two orders of magnitude by comparison with plasmas generated in a vacuum [21, 22]. The increase in the intensity of laser shock wave is achieved because the transparent confined layer prevents the generated plasma from expanding rapidly away from the surface. This results in more of the laser energy being delivered into the material as a shock wave [23].

For a Nd: glass laser with a wavelength of 1,054 nm, a transparent confined layer of water, quartz, or glass can increase the intensity of laser shock wave. These transparent confined layers are also known as overlays. The absorbing layer has also been found to increase the intensity of laser shock wave and to protect the metal's surface from laser ablation. Metallic absorbing layers have been found to be beneficial, if not necessary, to protect the component's surface [12]. Among the absorbing layers, commercially available Al foil has been found to be the most practical and effective, as compared to other absorbing layers.

When a laser pulse with enough intensity hits a metal target with an absorbing layer, the absorbing layer absorbs the laser energy, and vaporizes to form a plasma. Because of the ultra-short response times, the diffusion of thermal energy away from the interaction zone is limited to a couple of microns between the confined layer and the top surface of metal target and is preferred to be less than the thickness of the absorbing layer to maintain protection. This is important for alloys and metallic materials because laser ablation will reduce their fatigue lives [24].

The plasma keeps strongly absorbing the laser energy, and expanses in the confined region between the metal target and the transparent confined layer, and then creates a high amplitude, short duration pressure pulse. The shock wave induced by a portion of this energy propagates into the surface layer of alloys and metallic materials. When the peak pressure of the shock wave exceeds the dynamic yield strength of alloys or metallic materials, plastic deformation occurs, resulting in the improvement of the near-surface microstructure and mechanical properties consequently [25].

Some important factors need be taken into accounts when selecting the laser system for laser shock processing, such as cost, efficiency, reliability, and part replacement. Systems suitable for laser shock processing should have an energy output in the range of 10–500 J/pulse with pulse durations of less than 100 ns.

At present, the typical technology that can realize this type of energy output with an acceptable pulse length is a Q-switched laser system based on a Nd: glass or Nd: YAG crystal lasing rod which operates in the near infrared at a wavelength of 1,064 or 1054 nm and pulse duration of 10–100 ns.

2.4 Laser Shock Processing Equipment in this Book

In this book, we use two types of laser in the LSP experiment. One is a high-power and repetition-rate Nd: glass pulse laser developed by Laser Technology Institute and the University of Science and Technology of China in 2004, and the laser equipment and the light-road layout of laser head was shown in Fig. 2.1. The shock wave profile of a single laser pulse, and the output luminous field of a single laser pulse were shown in Figs. 2.2 and 2.3. This laser equipment can meet the demands of a single LSP impact and multiple LSP impacts, and its processing parameters were presented in Table 2.1.

The other is Nd: YAG laser manufactured by France Thales Company at Jiangsu University in China. Compared to the above laser equipment, this laser head has some advantages: (1) The Thales Company uses the unique design technology of Nd: YAG ceramic to ensure high stability; (2) Its tight structure and small size bring convenience when it is used; (3) It has a high repetition rate with 5 Hz to make the demand of industrial application. Structure layout of high-power Nd: YAG laser shock equipment manufactured by Thales Company was shown in Fig. 2.4.

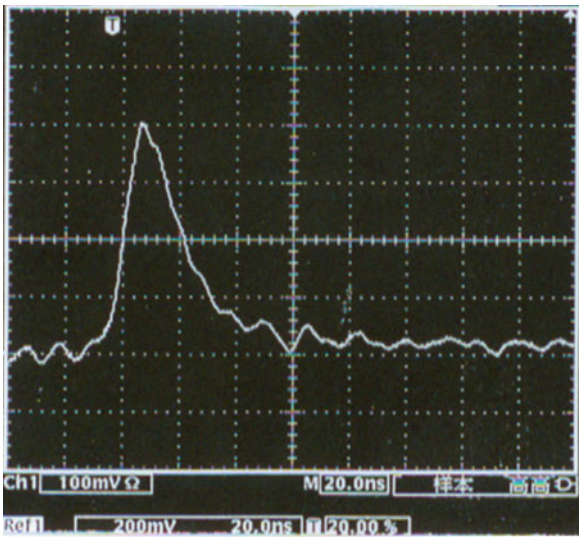

Fig. 2.2 Laser shock wave profile of a single pulse

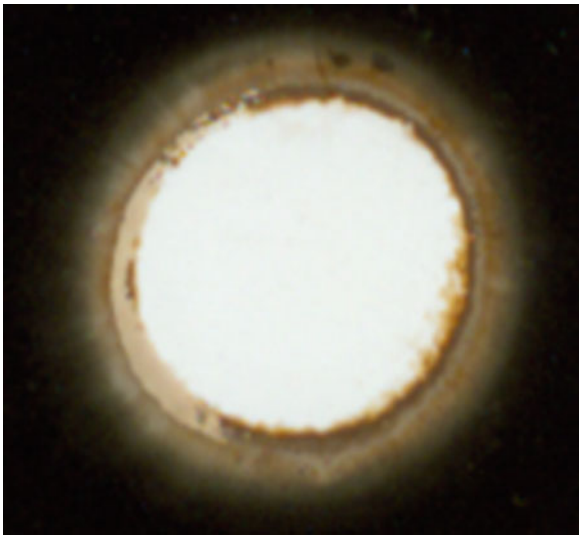

Fig. 2.3 Output luminous field of a single pulse

Table 2.1 Processing parameters of Nd: glass laser head

Type	Value
Beam div. of output (mrad)	≤0.5
Spot diameter (mm)	1–10
Pulse energy (J)	10–50
Repetition-rate (Hz)	1
Laser wavelength (nm)	1,054
Export stability	≤±5 %
Beam profile	Semi-Gauss

The system is composed of the following five parts: (1) A computer that controls the power supplies of the laser through the control unit and the ISEO delay generator; (2) The ISEO: 20 channels programmable delay generator; (3) 5 power supplies with a Control Unit for the Laser GAIA—R version; (4) One cooling unit; (5) The laser head which holds all the optical components. The light-road layout was shown in Fig. 2.5.

The output luminous field of a single laser pulse was shown in Fig. 2.6. This laser equipment can meet the demands of a single LSP impact and multiple LSP impacts, and its processing parameters were presented in Table 2.2.

During LSP, the effect of LSP depends on the processing position and the control of shock trace. To realize the accuracy and real-time control on the shock trace and the position between the workpiece surface and laser beam, the self-developed five-axis NC worktable with five degrees of freedom was used in the LSP experiments. The picture of 5-axis NC Worktable was shown in Fig. 2.7.

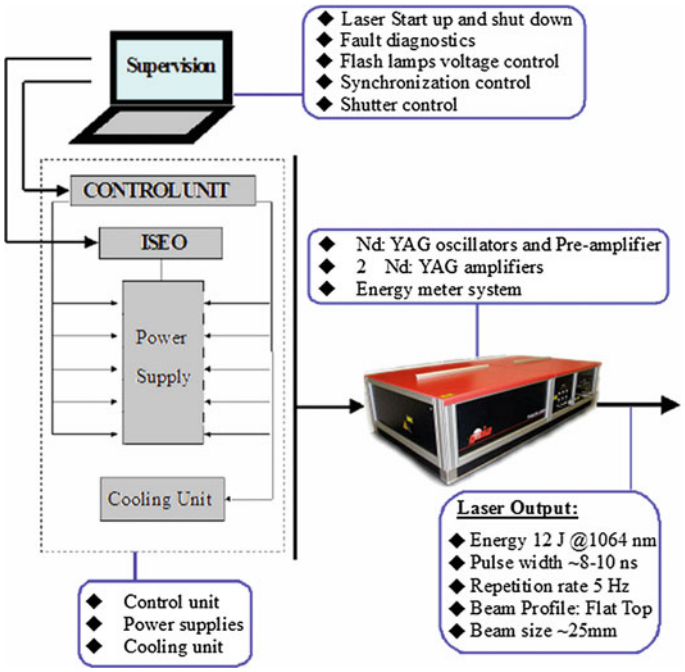

Fig. 2.4 Structure layout of high-power Nd: YAG laser shock equipment manufactured by Thales company

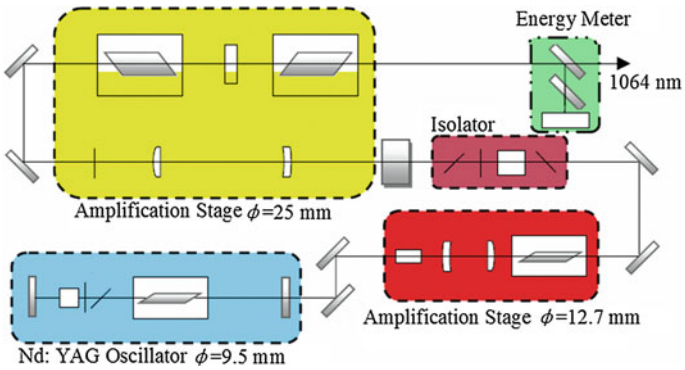

Fig. 2.5 Light-road layout of high-power Nd: YAG laser head

2.5 Nano-Hardness, Micro-Hardness and Residual Stress

After the development of high power laser, the laser surface modification of engineering materials draws a great deal of attention, which in turn causes rapid growth of fields of laser applications such as laser shock processing. The

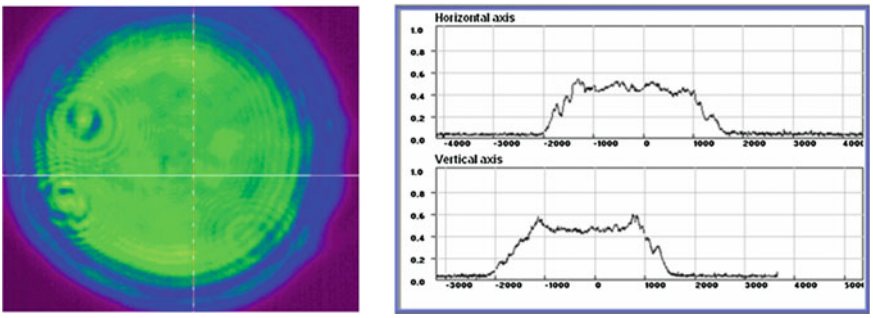

Fig. 2.6 Output luminous field of a single pulse

Table 2.2 Processing parameters of Nd: YAG laser head manufactured by Thales company

Type	Value
Beam divergence of output (mm. mrad)	≤2
Spot diameter (mm)	2–10
Pulse energy (J)	3–12
Pulse width (ns)	8–15 ns
Repetition-rate (Hz)	5
Laser wavelength (nm)	1,064
Beam profile	Top hat
Pulse to pulse energy stability (% rms)	<1.5 %

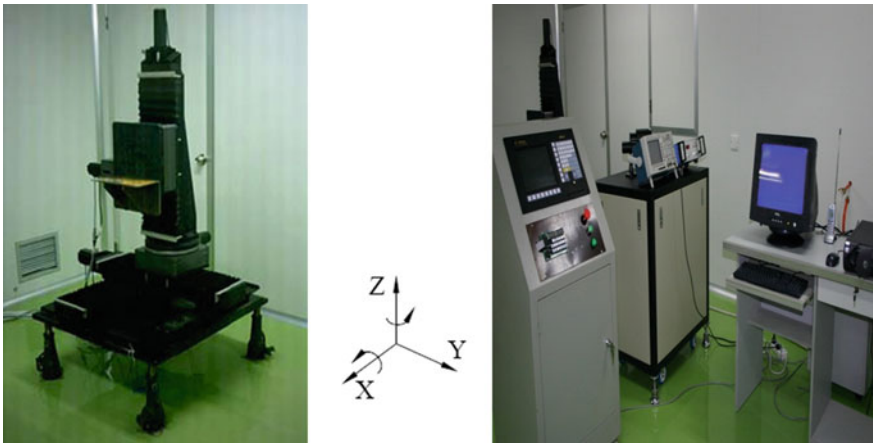

Fig. 2.7 Self-developed five-axis NC worktable with five degrees of freedom

magnitude of surface residual stress achieved by LSP is usually comparable to that achieved by shot peening, but the depth of compressive residual stress from LSP is significantly greater. Hence, many of the proposed applications of LSP are aimed

to improve the fatigue life and strength of the material through surface modification [26, 27].

Al alloy is widely used in aerospace and automotive industries due to its light weight and moderate strength. Considerable researches have been carried out to examine the effects of LSP on mechanical properties and fatigue lives of Al alloys [28–30]. Most of the above researches showed that the mechanical properties and fatigue lives were improved significantly for Al alloys due to the compressive residual stresses in the sample surface and in-depth direction after LSP. However, few studies have been focused on the effects of LSP on the nano-hardness and elastic modulus of Al alloy at the nanoscale. To the treated Al alloy by LSP, the reaction of the laser shock wave and the metal target will be generated near the target surface, leading to the generation of the dislocation and the microstructural deformation near the surface [31], and the increase in hardness was reported to be caused by an increment in the dislocation density with increasing laser impact repetitions [26]. The improvements of hardness and elastic modulus are correlated with the generation of the dislocation and the microstructural deformation near the surface [32] during LSP process, but no fundamental understanding in the LSP literature has been noted on the interaction of the microstructure with laser induced shock waves and the resulting changes in the microstructure. The majority of the reports on microstructural changes have been qualitative with few quantitative details such as dislocation density [33, 34]. The lack of a fundamental understanding on the strengthening mechanism of LSP on Al alloy by microstructure was most clearly reported. The effects of LSP on the nano-hardness and elastic modulus of Fe–Ni alloy were investigated by the nanoindentation techniques, but the mechanisms underlying the improved nano-hardness, elastic modulus and surface residual stress were only preliminarily addressed by evaluating the surface morphologies before and after LSP [35].

With the above background in mind, the purpose of this section was to examine nano-hardness and elastic modulus of LY2 Al alloy after LSP. In addition, the TEM analyses on the microstructures in the different regions after LSP were carried out, and the enhancement mechanism of LSP on nano-hardness and elastic modulus of LY2 Al alloy was also investigated and discussed. These topics discussed in this section will provide some important insights for researchers in the field of surface modification.

2.5.1 Experimental Material and Parameters

Some samples manufactured by LY2 Al alloy were cut into a rectangular shape with dimensions of $20 \times 20 \times 2$ mm^3. The chemical composition and mechanical properties of LY2 Al alloy were shown in Tables 2.3 and 2.4, respectively. Prior to the laser shock, the samples were polished with SiC paper with different grades of roughness (from 500–2,400), followed by cleaning in deionized water. Ultrasound

Table 2.3 Chemical composition of LY2 Al alloy

Composition	Cu	Mg	Mn	Si	Fe	Ti	Be	Cr	Zn	Al
Percent (wt %)	2.6–3.2	2.0–2.4	0.45–0.7	0.3	0.3	0.15	0.05	0.05	0.05	other

Table 2.4 Mechanical properties of LY2 Al alloy

Type	Value
Specific gravity, d, g/cm^3	2.8
Tensile strength, δb, kgf/mm^2	470
Elongation, δ, %	14
Vickers-hardness, HV	120

in ethanol was used to degrease the sample surface and LSP experiments were conducted shortly after preparation.

During LSP, the shockwaves were induced by a Q-switched Nd: glass repetition-rate laser with a wavelength of 1,054 nm, a pulse of about 20 ns, a diameter of 3 mm, and the laser energy was around 5 J, namely, laser power density is 9.7 GW/cm^2. A water curtain with a thickness of about 2 mm was used as a transparent confining layer and the professional Al foil with a thickness of 50 μm was used as an absorbing layer to protect the sample surface from thermal effect.

Transmission electron microscope (TEM) analyses on the microstructures of the different regions were performed on an H-800 TEM (*Hitachi Co., Japan*) with an accelerating voltage of 200 kV.

2.5.2 Measurement of Elastic Modulus and Hardness

Thin film mechanical properties (elastic modulus and yield strength) can be measured by tensile testing of freestanding films [36] and by the microbeam cantilever deflection technique [37], but the easiest way is by means of nanoindentation.

Here, no special sample preparation is required and tests can be performed quickly and inexpensively. Nanoindentation is similar to conventional hardness tests, while it is performed on a much smaller scale using special equipment. The force required to press a sharp diamond indenter into tested material is recorded as a function of indentation depth.

Both elastic modulus and hardness can be readily extracted directly from the nanoindentation curve. Since the depth resolution is on the order of nanometers, it is possible to indent even very thin (100 nm) films. A typical load–displacement curve of a 1 μm thick Cu film is shown in Fig. 2.8.

Elastic modulus is determined based on the knowledge of the tip shape function, and the load–displacement curve (load P and displacement h) [38].

The nano-hardness H and elastic modulus E_r were defined as follows:

$$H = \frac{P_{\max}}{A} \tag{2.1}$$

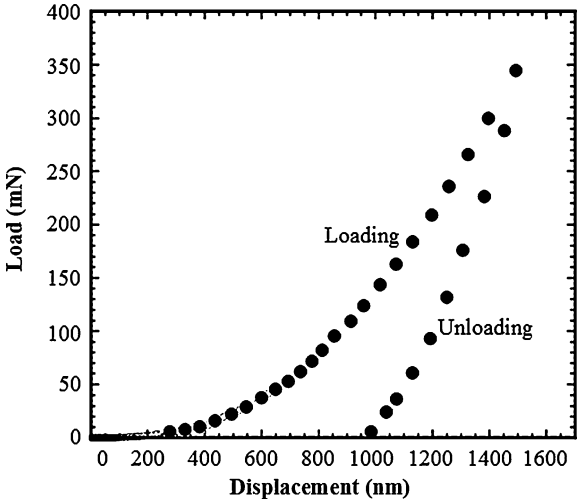

Fig. 2.8 Load–displacement curve for a 1 μm thick Cu film

$$E_r = \frac{\sqrt{\pi}}{2\beta}\frac{S}{\sqrt{A}} \tag{2.2}$$

here $P_{\max}$ is the maximum load, A is the projected contact area, S is the banner slope of unloading curve and β is the contact compliance between the indenter and the sample, which is equal to the tangent to the force–displacement curve during unloading after correction for frame compliance.

The symbols A and h_c in the Eqs. (2.1) and (2.2) are calculated as:

$$A = 24.56h_c^2 + \sum_{i=0}^{7} C\beta h_c^{1/2^i} \tag{2.3}$$

$$h_c = h - \beta P_{\max}/S \tag{2.4}$$

where h_c is the contact depth and h is the indention depth, as shown in Fig. 2.9.

The other experimental conditions of nano-indentation are: (1) Depth limit 3,000 nm; (2) Strain rate target 0.05 s^{-1}; (3) Maximum calculation depth 2,500 nm and (4) Minimum calculation depth 1,000 nm.

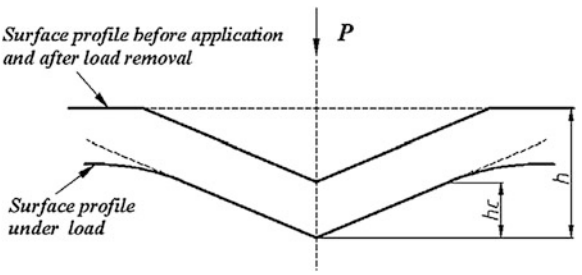

Fig. 2.9 Definition of depth hc and h in the indentation test

2.5.3 *Effects of LSP on Nano-Hardness and Elastic Modulus*

Figure 2.10a, b, c showed the measured load–displacement curves for the non-shocked region, the laser-affected region and the laser-shocked region at a maximum load of 960 μN, respectively. P_{max}, A, S and h_c were calculated during unloading by using Eqs. (2.1–2.4), and the measurements were repeated five times for each condition, an average value was determined on the basis of the five measured data. The corresponding experimental data were shown in Table 2.4. It can be found that the contact depths of the indenter were 247.58, 196.07 and 150.51 nm in the non-shocked region, the laser-affected region and the laser-shocked region, respectively. The maximum contact depth of the indenter at peak load decreased gradually from the non-shocked region to the laser-shocked region.

The measured values of nano-hardness near the surface in different regions were shown in Fig. 2.11a. It can be seen that the values of nano-hardness in the laser-shocked region and the laser-affected region were improved obviously in comparison with the corresponding values in the non-shocked region. The experimental data about nano-hardness H were also shown in Table 2.5 in detail. Firstly, it can be seen from Table 2.4 that in the non-shocked region, i.e., the untreated material, the nano-hardness kept a constant value of 0.535 GPa;

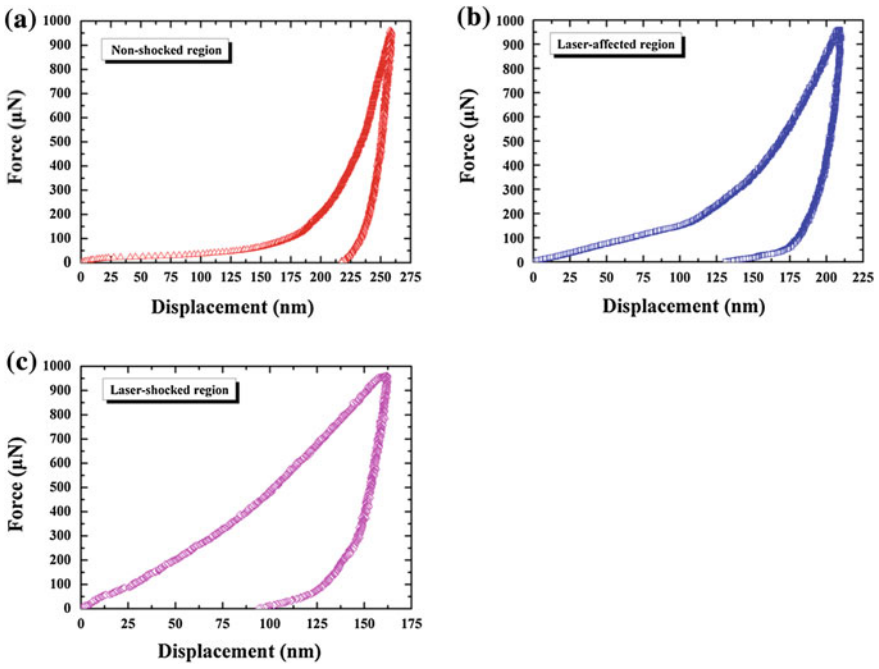

Fig. 2.10 The measured load-displacement curve at a maximum load of about 960 μN in the indentation test. **a** In the non-shocked region, **b** in the laser-affected region, **c** in the laser-shocked region

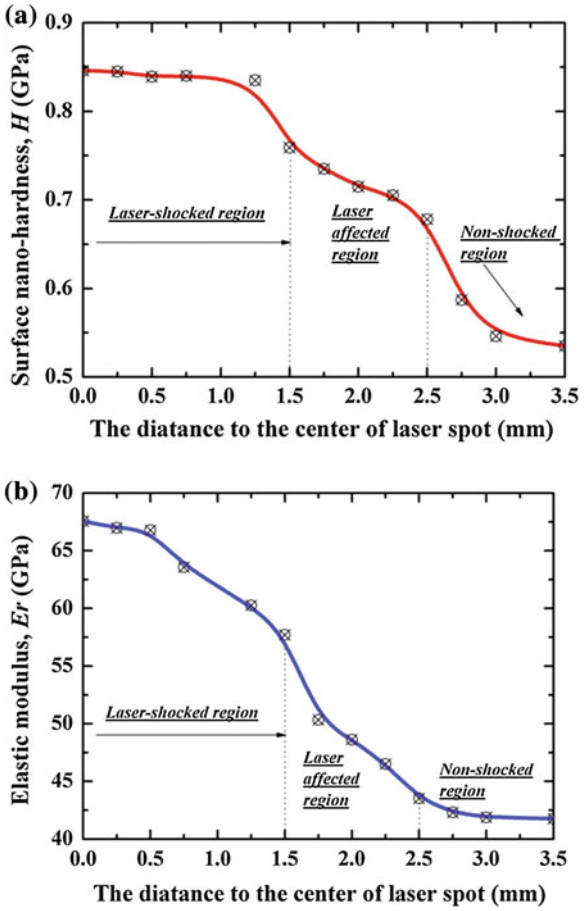

Fig. 2.11 The measured values near the surface in different laser treated regions in the indentation test. **a** nano-hardness, **b** elastic modulus

Table 2.5 The values of nano-hardness and elastic modulus in different regions

	Non-shocked region	Laser-affected region	Laser-shocked region
Maximum load, P_{max}/μN	960	960	960
Contact depth, h_c/nm	247.58	196.07	150.51
Contact area, A/nm^2	1,142,091	1,381,584	1,783,028
Slope, S/μN·nm^{-1}	47.23	61.74	72.95
Nano-hardness, H/GPa	0.535	0.718	0.846
Elastic modulus, E_r/GPa	41.77	50.33	67.56

Secondly, nano-hardness reached about 0.718 GPa in the laser-affected region, which was greater by 34.2 % than that in the non-shocked region; Lastly, when it got into the laser-shocked region, nano-hardness value was 0.846 GPa, which was greater by 58.13 % than that in the non-shocked region after LSP treatment.

The values of elastic modulus in different regions were obtained according to Eq. (2.2) on the basis of the obtained value of A, S and β, which were also shown in Table 2.4. It can be seen that the value of elastic modulus was 41.77 GPa in the non-shocked region, and the corresponding value was 50.33 GPa in the laser-affected region, while 67.56 GPa in the laser-shocked region, respectively. Obviously, the values of elastic modulus in the laser-affected region and the laser-shocked region were increased by 20.49 and 61.74 % compared to that in the non-shocked region, respectively. Figure 2.11b showed that the magnitude of elastic modulus decreased from the laser-shocked region to the non-shocked region, and it was clear that the values of elastic modulus in the laser-shocked region and the laser-affected region were obviously greater than those in the non-shocked region.

Although the elastic modulus is an intrinsic material property and fundamentally related to atomic bonding, it can be changed by some surface treatment technologies. The elastic modulus of 304 SS samples by the high-energy shot peening and ultrasonic shot peening shows an obvious fluctuation along the depth profile [39]. The elastic constant C44 and shear modulus of the Al alloy 2024-T62 subjected to LSP decrease by up to 29.0 and 25.4 %, respectively. The values of elastic modulus in the laser-shocked region and the laser-affected region were clearly greater than those in the non-shocked region. It is well known that the increment of elastic modulus is advantageous in enhancing the stiffness of the parts, which determines their stability when the components are applied in environment [40]. Hence, it can be concluded that LSP can improve the stiffness of the samples manufactured by the LY2 Al alloy.

The resistance of foreign object damage (FOD) depends strongly on the stiffness of the component [41] and the most important material parameter affecting FOD was identified as hardness of the surface material [42]. From the above experimental data, it can be seen that the values of nano-hardness in the laser-shocked region and the laser-affected region were greater than those in the non-shocked region. As a consequence of the lower contact depth in the laser-shocked region compared to that in the non-shocked region, the values of nano-hardness in the laser-shocked region were greater from another point of view. When shock wave pressure was higher than approximately 5 GPa, LSP can produce the increments of surface hardness over the entire laser irradiated area, such as the hardness of underaged 2024-T351 [43] and 6061-T6 [44]. The above research results were also in good agreement with those obtained by Montross et al. [45]. Therefore, LSP can improve the nano-hardness and elastic modulus of sample surface layer, which was favorable for improving FOD resistance of the components manufactured by LY2 Al alloy.

2.5.4 Enhancement Mechanism of LSP on Hardness and Elastic Modulus

Figure 2.12a, b showed the TEM micrographs of sample surface with the laser power density of 9.7 GW/cm^2 in the non-shocked region and in the laser-shocked region, respectively. It can be seen from Fig. 2.5a that there were plenty of grains with the average dimensions of 130 × 130 nm^2 and a small amount of dislocations in the non-shocked region. In the laser-shocked region, the grains were clearly refined to be the smaller grains with the average dimensions of 60 × 60 nm^2, and there were plenty of dislocation tangles in the vicinity of grain boundaries. In addition, a small amount of twins were also found (which were demonstrated by the rectangulars A, B and C). Figure 2.12c was the high magnification micrograph of the twins of the rectangular A in Fig. 2.12b.

Micro-mechanism of the metal plastic deformation is a generation and motion of dislocation, and the metal plastic deformation ε can be expressed by the Orowan's relation [46], i.e.

$$\varepsilon = K\rho\chi b \tag{2.5}$$

where ρ was dislocation density, K was a factor that was concerned of dislocation, b was the scalar value of Burgers vector, and χ was the average distance of dislocation.

According to the previous work [47], mechanical properties, such as hardness and yield stress, can be expressed in terms of microstructure, such as dislocation

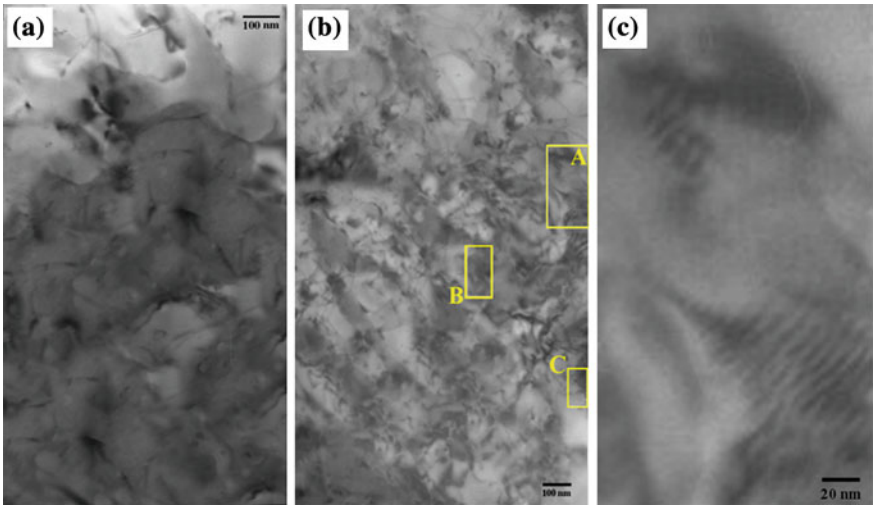

Fig. 2.12 (**a**) and (**b**) is respectively the TEM micrographs of sample surface with laser power density of 9.7 GW/cm^2 in the non-shocked region and the laser-shocked region, and (**c**) was the magnification TEM micrograph of the twins of the *rectangular A* in (**b**)

density and twin spacing. In the present study, the dislocation substructure was the key feature observed in the laser-shocked region of LY2 Al alloy. The measured surface nano-hardness, H, can be described by the following equation,

$$H = H_0 + aGb\sqrt{\rho} \tag{2.6}$$

where H_0, a, G, and b are the material's constants. H_0 is the surface nano-hardness of an ideal material without any defects, G is the shearing modulus; and a is the constant which has relation to crystal structure. As an approximation, the material's constants a, G, and b are calculated based upon the results obtained by Ganin et al. [48]. In the present study, LY2 Al alloy was explosively shock loaded at 3.14 GPa and nano-hardness values are taken on sample surface in different regions.

The microstructural changes occurred in the alloy during LSP, and the plastic deformation were a direct consequence of the change of grain size and dislocation density and the rearrangement of dislocations. The reaction between laser shock wave and the metal target will be generated near the target surface after LSP, leading to the increment of the dislocation density and the microstructural deformation near the surface [49]. LSP caused plastic deformation of the sample surface which was recessed by several microns due to this plastic deformation, and high density dislocations and a small amount of twins were observed in the TEM micrographs. Therefore, it was reasonable to conclude that the strengthening of LSP on the mechanical property of LY2 Al alloy was mainly due to the generation of high density dislocations after LSP.

2.6 Surface Roughness and Surface Profile

Surface roughness plays a highly important role on fatigue lives of alloys [50, 51]. The previous studies very little involve the fully investigation of surface topography about LSP treatment [52–54]. Zhang et al. [52] investigated the surface qualities of LSP zones to the fatigue life of Al alloy. They found that the fatigue life decreased with the increase of surface roughness. Chu and Rigsbee [47] found that the surface roughness of low carbon steel increased with the increase of laser shock pressure. Rozmus [53] found the surface roughness of Ti6Al4 V Alloy increased from 0.1–0.82 μm after LSP treatment. However, the research of Zhang and Lu [33] indicated that the surface roughness of LY2 Al alloy decreased obviously after LSP treatment. The reason caused the difference of conclusion was that they all did not consider the effect of initial surface topography to the results of LSP treatment. Additionally, the effect of initial surface topography to the residual stress and micro-hardness has also not been discussed.

Different mechanic methods will produce different kinds of surface topography and corresponding typical features. It is important to understand the evolution of these typical features because their existence will acquire different results as

treated by LSP. In this study, LY2 Al alloy samples with four different initial surface conditions were prepared. The surface topography was carefully investigated before and after LSP treatments. In addition, the surface residual stress and micro-hardness were also studied. These studies can provide more clues with regarding to fatigue lives of LY2 treated by LSP.

2.6.1 Sample Preparation and Surface Topography Measurements

The samples of LY2 were cut into rectangular plates with dimensions of 10 × 10 mm and a thickness of 5 mm, and then they were mounted on a motor controlled by x − y stage with 1 μm of resolution and maximum speed of 20 mm s^{-1}. Four different initial surface conditions were conducted as following: 1 burnished with #150 SiC paper, 2 burnished with SiC paper with different grades of roughness (from #150 to #600), 3 burnished with SiC paper with different grades of roughness (from #150 to #1,200), 4. burnished with SiC paper with different grades of roughness (from #150 to #1,200), then polished with silk. Before and after LSP, ultrasound treatment in ethanol was used to clean the surface of all the tested samples.

LSP experiments were conducted shortly after the preparation of LY2 samples. LSP experiments were performed using a Q-switched Nd: YAG laser operating at 5 Hz repetition rate with a wavelength of 1,064 nm, and the full width at half maximum (FWHM) of the pulses were about 10 ns. The laser beam was focused by a focal lens and the spot diameter was about 3 mm when it arrived at the to-be treated samples. A water layer with a thickness of about 1 mm was used as the transparent confining layer and a professional black polyester tape with a thickness of 180 μm was used as the absorbing layer. The laser pulse energy was 6 J. During multiple LSP impacts, the laser beam was perpendicular to the same location on the sample, and the black polyester tape was replaced after each impact.

Surface topography was test by a Veeco Wyko NT 1,100 non-contact optical profiler (NCOP). The Wyko Vision software is the heart of the optical profiler measurement system. It provides powerful measurement and analysis capabilities, with over 200 analysis tools including 2D and 3D plots, histograms, and many application-specific tools and parameters, including surface height statistics such as Rp, Rv, Rt Rq, and Ra [55]. In this section, the tested area was a 240 × 180 μm rectangle at the center of laser spot.

2.6.2 Surface Topography

Figures 2.13a1, a2, a3 show the 3D surface topography of #150 samples before LSP, by one LSP impact and by three LSP impacts respectively. In Fig. 2.13, #150 and Un represents the sample burnished with #150 SiC paper before LSP, #150 and One LSP represents the sample burnished with #150 SiC paper then subjected to one LSP impact and #150 and Three LSP represents the sample burnished with #150 SiC paper then subjected to three LSP impacts, respectively. The corresponding 2D topography is shown in Fig. 2.14. Compared with #150 and Un (Fig. 2.13a1), #150 and One LSP (Fig. 2.13a2) and #150 and Three LSP (Fig. 2.13a3), it can be seen that the features marked with circle disappear gradually. The characteristic of these gradually disappeared features can be seen in Fig. 2.14. The height-width ratio for these kinds of features is high (more than 2). These features are named sharp protruding here. However, it can be seen that the features marked with parallelogram always exist even after three LSP impacts. The typical characteristic of these features is micro groove.

In order to find out the detailed statistical data of examined surfaces, the number of data points at each surface height is shown Fig. 2.15. The sampling of surface height is dependent on the Wyko Vision software automatically. It can be seen from Fig. 2.15a that the number of data points whose height exceeding 4 μm decreases gradually after LSP. The surface height distribution of #150 and Un scatters from −5–15 μm, and it is narrowed effectively after one LSP (from −5–4 μm).

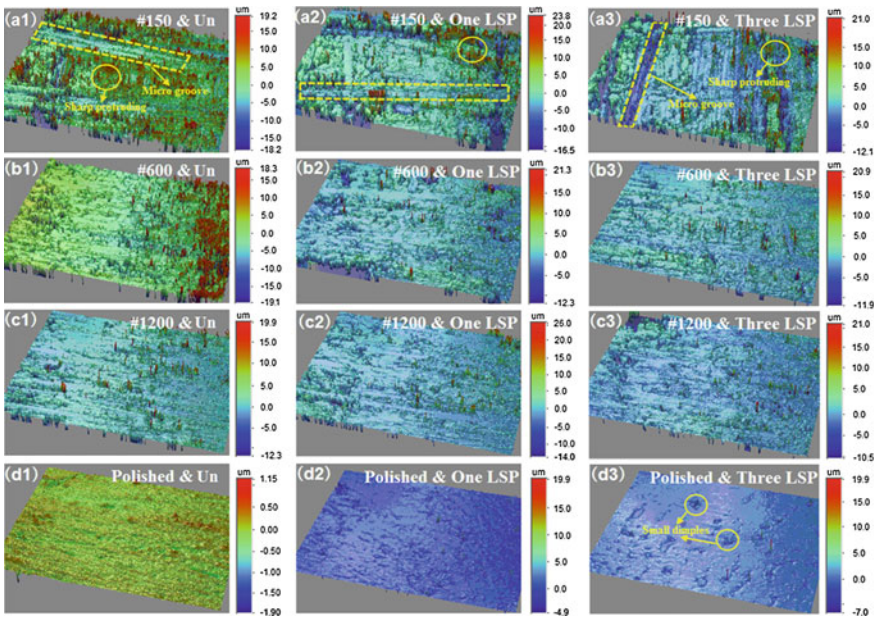

Fig. 2.13 3D surface topography of LY2 Al alloy treated by LSP

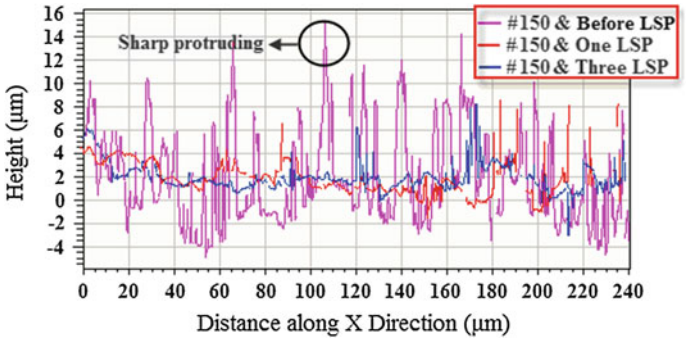

Fig. 2.14 2D surface topography of LY2 Al alloy burnished with #150 SiC paper

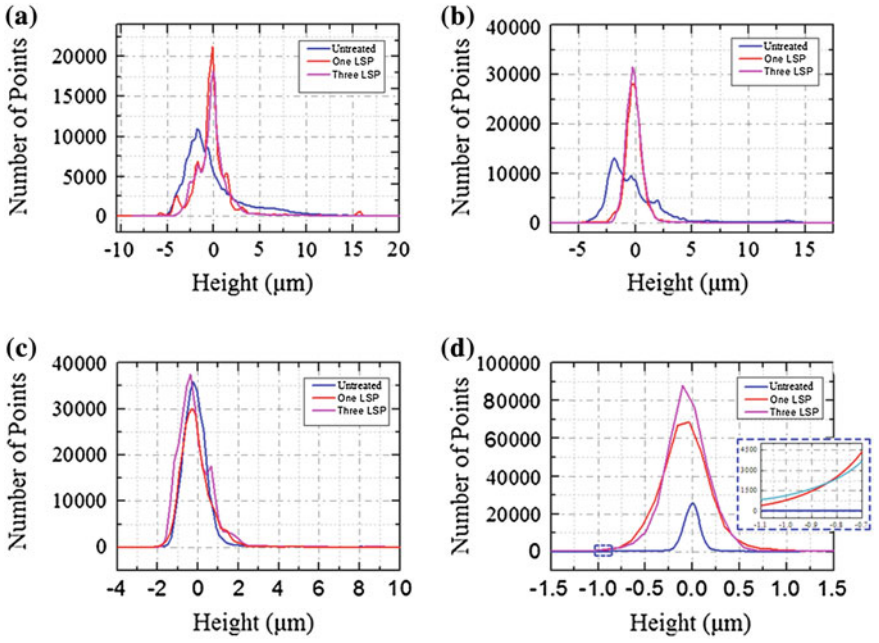

Fig. 2.15 Histogram showing the number of data points at each surface height. **a** burnished with #150 SiC paper, **b** burnished with #600 SiC paper, **c** burnished with #1,200 SiC paper, **d** polished with silk

When subjected to three LSP impacts, there is hardly change for surface height distribution.

The surface height of #600 and Un (Fig. 2.15b) scatters from −5 to 5 μm, while it scatters from −2.5 to 2.5 μm after one LSP. When subjected to three LSP impacts, it has a little change (from −2.0 to 2.5 μm). The surface height distribution of #150 and One LSP and #600 and Un is almost similar, but the results are

different when subjected to one more LSP impact. This is because the dominant features of #150 and One LSP is micro groove while that of One LSP and #600 and Un is sharp protruding.

Figure 2.15c shows that the surface height distribution of #1,200 is widened a little after LSP, and it is not very obvious. After three LSP impacts, the surface height distribution of #1,200 sample scatters from −2.0 to 2.5 μm, which is similar to the #600 and Three LSP. This indicates that their ultimate surface condition may be the same after LSP impacts although the initial surface height distribution is quite different.

Figure 2.15d shows that the surface height distribution will be enlarged rapidly (from −1.0 to 1.0 μm) after one LSP impact when the surface is very smooth (from −0.4 to 0.4 μm). When subjected to three LSP impacts, it seems that there is a little difference compared with one LSP impact. However, the left partial enlarged view shows that the number of points below −0.85 μm increases after three LSP impacts. The small dimples formed in Fig. 2.15d3 can explain this phenomenon.

Figure 2.16 shows the surface roughness of all the tested samples. The surface roughness is an average value of all the statistical points' surface height, which are sampled by the Wyko Vision software. The surface roughness R_a of #150 sample decreases from 2.45 to 1.47 μm after one LSP impact. When subjected to three LSP impacts, the surface roughness is 1.42 μm, indicating that multiple LSP impacts cannot decrease surface roughness obviously any more. This tendency can be seen on the surface roughness for all the other samples. The surface roughness of #600 sample decreases from 1.88 to 0.59 μm after one LSP impact and to 0.58 μm after three LSP impacts. Zhang et al. [52] found the surface roughness of some of their 2024-T72 Al alloy samples decrease from 3.2 to 1.6 μm after LSP treatment, but some others increase from 3.2 to 6.4 μm, even to 12.5. The unstable LSP process may be the main reason. The surface roughness of #150 and One LSP is much higher than that of #600 and One LSP. This is because there are plenty of micro grooves (Fig. 2.13a3) on the surface of #150 sample, while no micro groove exists on the surface of #600 sample.

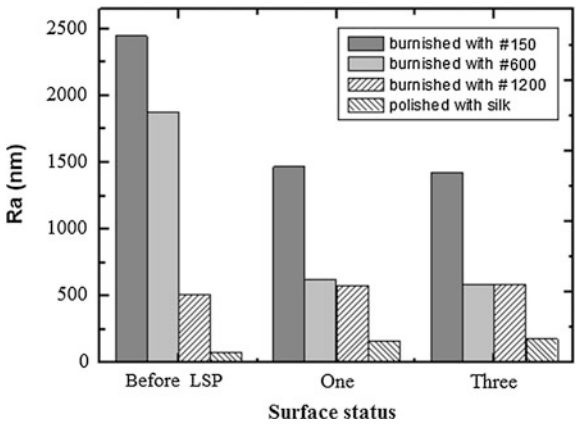

Fig. 2.16 Comparison of surface roughness with different surface status

However, the surface roughness of #1,200 sample increases from 0.49 to 0.56 μm after one LSP impact and to 0.58 μm after three LSP impacts. Although the initial surface roughness is quite different, the surface roughness of #600 and Three LSP is equal to that of #1,200 and Three LSP. These imply that there is an ultimate value about surface roughness of LY2 in the present experimental conditions. Similar results could be found in the works of Luong et al. [26]. They found the surface roughness of 7085-T7651 Al alloy increased from the initial 0.444 to 0.518 μm after three LSP impacts. Rozmus-Górnikowska et al. [56] found the roughness of Ti6Al4 V Alloy increased from 0.1 μm before treatment to 0.82 μm after LSP impact. All these results indicate that there is some ultimate value about surface roughness surface roughness for the alloys treated by LSP, but their ultimate values are different from each other. The reason of this phenomenon may be the difference and parameter of LSP treatment mechanical performance of alloys.

For the polished sample, the surface roughness of sample before LSP is double that of one LSP impact, and then a very small increment is obtained when subjected to three LSP impacts. It can be seen that small dimples (Fig. 2.13d3) form when subjected to three LSP impacts, which will certainly enhance the surface roughness. So the surface roughness of polished sample can be continuously increased. Similar result also could be found in the study of Chu et al. [47], in which they found the increase of surface roughness when a polished sample of low carbon steel is subjected to LSP impact. The underlying reason for the increase of surface roughness may be due to the unevenness of absorbing layer. Figure 2.17 shows the schematic principle of this phenomenon. Here, the surface of alloy is assumed to be flat. When laser shock wave propagates into the air between the Al foil and alloy, it will attenuate. Obviously, this will cause the intensity difference of laser shock wave on the surface of alloy at different positions. The intensity difference of laser shock wave will certainly bring the increase of surface roughness.

It may be the fact that after enough number of LSP impacts, when the vanishing of sharp protruding and the production of small dimples caused by the un-uniform of laser intensity reach to a balance, the surface roughness reaches its ultimate value. Here the ultimate value is 0.58 μm.

For the #150 sample, it can also be reasonably concluded that the surface roughness will reach to 0.58 μm when subjected to enough number of LSP impacts at a same point. However, it is not economical in industrial production as to multiple LSP impacts.

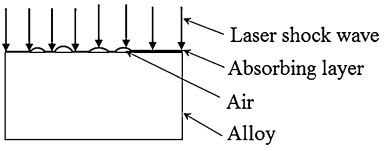

Fig. 2.17 Schematic illustration of the increase of surface roughness generated by laser shock processing

2.6.3 Residual Stress

Because the residual stress is different everywhere along the radial direction [57] within a same laser spot when treated by LSP, all the tested points locate in the center of laser point to make a suitable comparability. Figure 2.18 shows the tested surface residual stress of all the samples. The surface residual stress of #150, #600, #1,200 and polished sample is −58, −133, −146 and −149 MPa respectively when subjected to one LSP impact. This indicates that the increasing surface roughness will decrease the compressive residual stress. When subjected to three LSP impacts, the surface residual stress of all the samples are almost the same (about −150 MPa). It can be concluded that the residual stress tends to be saturated when subjected multiple LSP impacts and the saturated compressive residual stress is independent of surface roughness.

2.6.4 Micro-Hardness

The surface micro-hardness is also different everywhere [58] on the scope of same laser spot, which is similar to the distribution of residual stress. In order to ensure good comparability of the results, the testing points of micro-hardness are around the center of laser spot. Figure 2.19 shows the surface micro-hardness of all the tested samples. The micro-hardness of all the samples before LSP is about the same. It is obvious that LSP can improve micro-hardness. After one LSP impact, the micro-hardness decreases with the decrease of surface roughness. The reason may be described as Fig. 2.20: LSP will cause sharp features to vanish, and these features will experience much more severe deformation than the flat surface. This reinforces work-hardening effects and causes the increase of micro-hardness. After three LSP impacts, the micro-hardness of all the tested samples increases slightly. The increase of micro-hardness is due to the increase of dislocation density, this

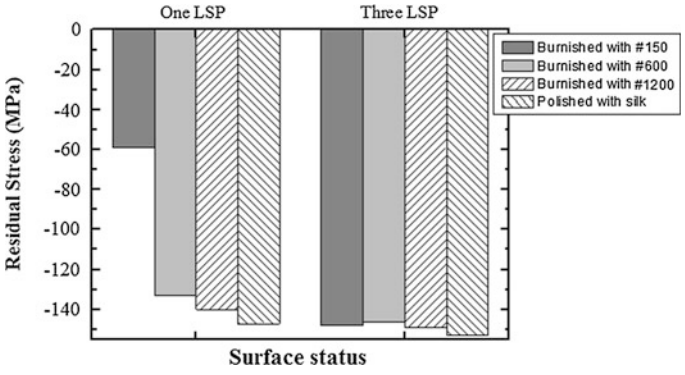

Fig. 2.18 Comparison of surface residual stress with different surface status

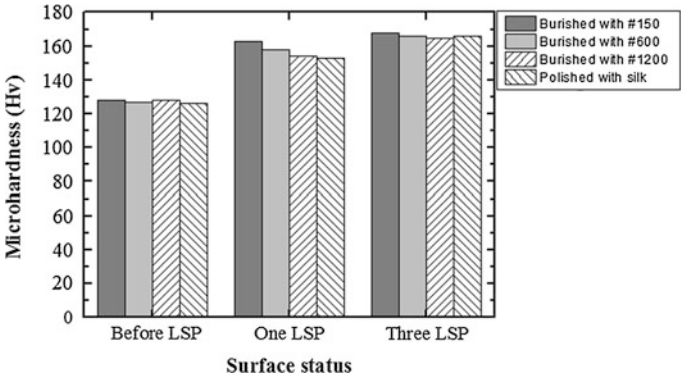

Fig. 2.19 Comparison of surface micro-hardness with different surface status

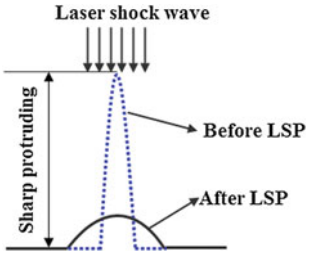

Fig. 2.20 Schematic of plastic deformation with sharp protruding

has been proved in the work of Clauer et al. [59]. However, the micro-hardness of all the samples is almost equal after three LSP impacts. This implies that the initial surface topography has no influence on the micro-hardness of LY2 after multiple LSP impacts.

2.7 Simulation and Validation of the Residual Stresses Using Laser Elliptical Spot

Among the laser surface treated methods, the laser shock processing (LSP) is a new and promising surface treatment technique to improve the fatigue, corrosion and wear resistance and the mechanical properties of the metals and alloys through generating this shock wave and introducing the deep compressive residual stresses into the materials [60–67]. Hence, many of the proposed applications of LSP are aimed to improve the fatigue life and strength of the material through surface modification [68, 69].

Warren et al. [67] performed finite element method (FEM) simulations of LSP Al(Al) alloy in single and multiple passes by using the developed spatial and temporal shock pressure model. The study results indicated that high residual

compressive stress was developed in the deformed region [22], which improved the surface properties of the Al alloy. And the predictions of the FEM analysis [70] agreed well with the experimental data of the multiple LSP impacts. Hu et al. [71] have performed three-dimensional (3D) FEM analysis on the residual stresses due to multiple LSP, and the effects of different overlapping rates and impact sequences on the distribution of residual stresses were also simulated. Some experimental results were presented to examine the mechanical properties of metal samples after LSP [72, 73].

The above studies have focused on the determination and simulation of residual stress and hardness distributions at the surface and subsurface by LSP with round spot. It is well known that different laser spot profiles can induce different shock effects, and the different spot profiles can also be applied according to different requirements during LSP. A laser beam with a round profile was extensively used due to the work matter of the laser, and a laser beam with a square profile allowed dense, uniform packing of the laser spots [71], the distribution of residual stresses by LSP with square spot was investigated in the literatures [74, 75], which was different compared with that with round spot. Clauer et al. [76] focused on the effect of LSP on the fatigue crack growth of pre-existing cracks of the samples with a centered hole, using different laser spot profiles, such as annular spot and round spot. The results showed that the 2024-T3 samples treated with the round laser spot had a fatigue life about 13 times longer than the ones with the annular laser spot. Meanwhile, there is another laser spot profile, i.e., elliptical spot, which is easily modulated and has been applied for long edges of metal parts. However, LSP with elliptical spot is rarely investigated.

The aim of this section was to investigate the effect of laser shock processing with elliptical spot (long-axis length 12 mm and the short-axis length 3 mm) on the residual stress distribution of LY2 Al alloy samples. Residual stress was investigated with different overlapping rates. A FEM model was developed to simulate the distribution of residual stress during the overlapping process by using ABQUAS software. The simulated residual stress field was analyzed and compared with the experimental results. The relations between the magnitude and uniformity of residual stress and the overlapping rate were also addressed. These discussed topics could give some important insights on the surface treatment and life-extension of long edges of metal parts.

2.7.1 Sample Preparation and Measurements of Residual Stress

The LY2 Al sheet was cut into a rectangular shape with $30 \times 15 \times 10$ mm^3 (width $\times$ length $\times$ thickness). The grinding and polishing were performed across the sample surfaces, and then the samples were cleaned ultrasonically before the experiments.

In LSP, the shockwaves were induced by a Q-switched repetition-rate laser with a wavelength of 1,054 nm and a pulse of around 20 ns. The water with a thickness of 1–3 mm was used as the transparent confining layer and the 7,075 Al foil with a thickness of 100 um was used as an absorbing layer to protect the blade surface from thermal effect. Laser energy was around 40 J. The deformed surface layer is loaded in compression by the undeformed bulk material as shown in Fig. 2.21a, b.

Five samples by LY2 Al alloy were treated by using the same experiment condition, and the schematic diagram of the shocking path by LSP with elliptical spot was shown in Fig. 2.22.

The residual stresses at the surface of the sample and through the depth direction after LSP were determined by using x-ray diffraction. For the measurement of the residual stress in depth direction, the electropolishing material removal method was used. The experiment was carried out with overlapping LSP. The experiments were repeated five times, and the experimental data are the average value of five samples.

2.7.2 Numerical Simulation Procedures

The commercial FEM software ABAQUS [77] was used to predict the residual stress and strain distribution at the surface and subsurface of the metal target during and after LSP. As most of the laser impacts were elliptical, a plane

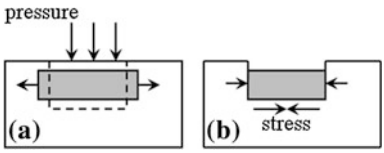

Fig. 2.21 Residual stresses pattern during (**a**) and after (**b**) the interaction

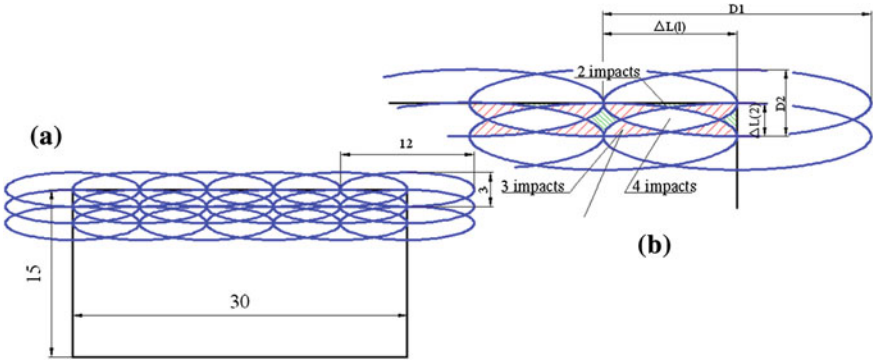

Fig. 2.22 Schematic diagram of the shocking path by LSP with elliptical spot when the long-axis length is 12 mm and the short-axis length is 3 mm

symmetric problem was chosen in order to reduce the data processing time. C3D8R (continuum, 3 dimensional, eight nodes, and reduced integration) was used in the FEM. The symmetric boundary condition was employed on the XOZ plane of the 3D finite element area. The FEM analysis procedure of LSP should be composed of two distinct parts [78], namely dynamic analysis and static analysis to capture an absolutely stable residual stress field and the elasto-plastic surface deformation.

In the present work, the residual stresses subjected to the single and multiple LSP with elliptical laser spots was considered in the experimental investigation and the FEM analysis. The material properties were listed in Table 2.4. LSP generated strain rate at the surface of the target exceeding $10^7\ s^{-1}$. The elastic limit stress in the direction of the shock wave propagation was defined as the Hugoniot Elastic Limit (HEL) [70]. When the peak pressure in the direction of the wave propagation is greater than HEL, plastic deformation occurs. The relationship between the dynamic yield strength, σ_y^{dyn}, and HEL under uniaxial strain conditions can be defined as

$$\sigma_y^{dyn} = \mathrm{HEL}\frac{1-2v}{1-v} \tag{2.7}$$

where v is the Poisson's ratio. The plastic strain was assumed to follow the von Mises yielding criterion in which the dynamic yield strength was defined as above.

Overlapping rate η in two directions is defined to describe and control the distribution of laser pulses on the impact region, which is expressed as

$$\eta = \frac{\Delta L}{D} \tag{2.8}$$

where ΔL is the coincidence length of overlapped two successive laser spots and D is the long-axis length or the short-axis length, as shown in Fig. 2.22. η_L and η_S is the overlapping rates in the long-axis (X) direction and the short-axis (Y) direction respectively. The output pulse energy 40 J and elliptical spot (long-axis length 12 mm and the short-axis length 3 mm) were selected with overlapping rates $\eta_L = 30$, 50 and 70 % in the simulation and experiment. In the present work, the residual stress S11 along long-axis (X) direction was considered.

2.7.3 The Simulation and Verification of Surface Residual Stress Distribution

The benchmark simulation is to verify that the single and multiple impacts of LSP simulation produced similar residual stress magnitudes and distributions as experimentally observed by Yakimets et al. [79]. The benchmark simulation consisted of a single LSP located at the center of the workpiece as shown in Fig. 2.23, and the simulation condition is also shown in Fig. 2.23. The benchmark

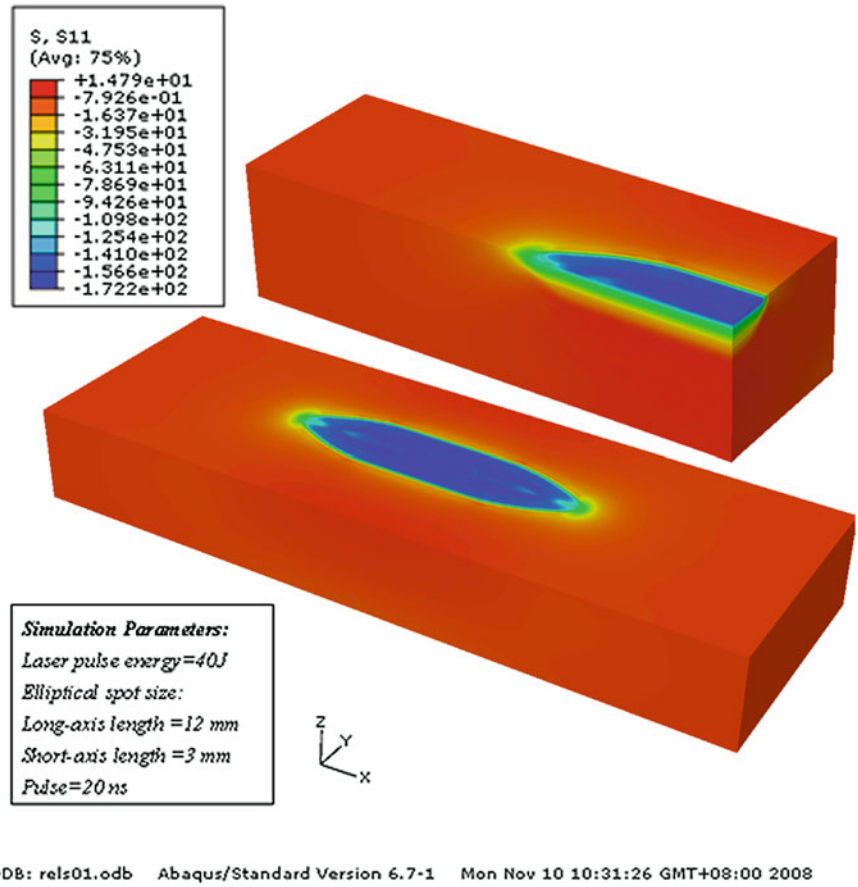

Fig. 2.23 Benchmark simulation model of single LSP

simulation mesh consisted of C3D8R-type elements. Elements size is biased with a higher density of elements near the surface and gradually becoming less dense with increasing depth below the surface. The initial values of residual stress S11 were approximate in the zero-stress state.

Simulations were successively conducted with another two laser shocks on one side of the first treated zone by 30, 50 and 70 % overlapping rate along X direction. Figure 2.24 showed the distribution of surface residual stress S11 for different overlapping rates in the simulation with initial stress removed. The simulated residual stress distributions in the surface layer were given in Figs. 2.25a, b, and Fig. 2.25b was the enlarged partial view in overlapped regions. As shown in these figures, following observations can be made when compared with a single LSP impact.

The maximum magnitudes of compressive residual stress on the top surface were about -172 MPa for the first impact. However, it was greatly increased, after

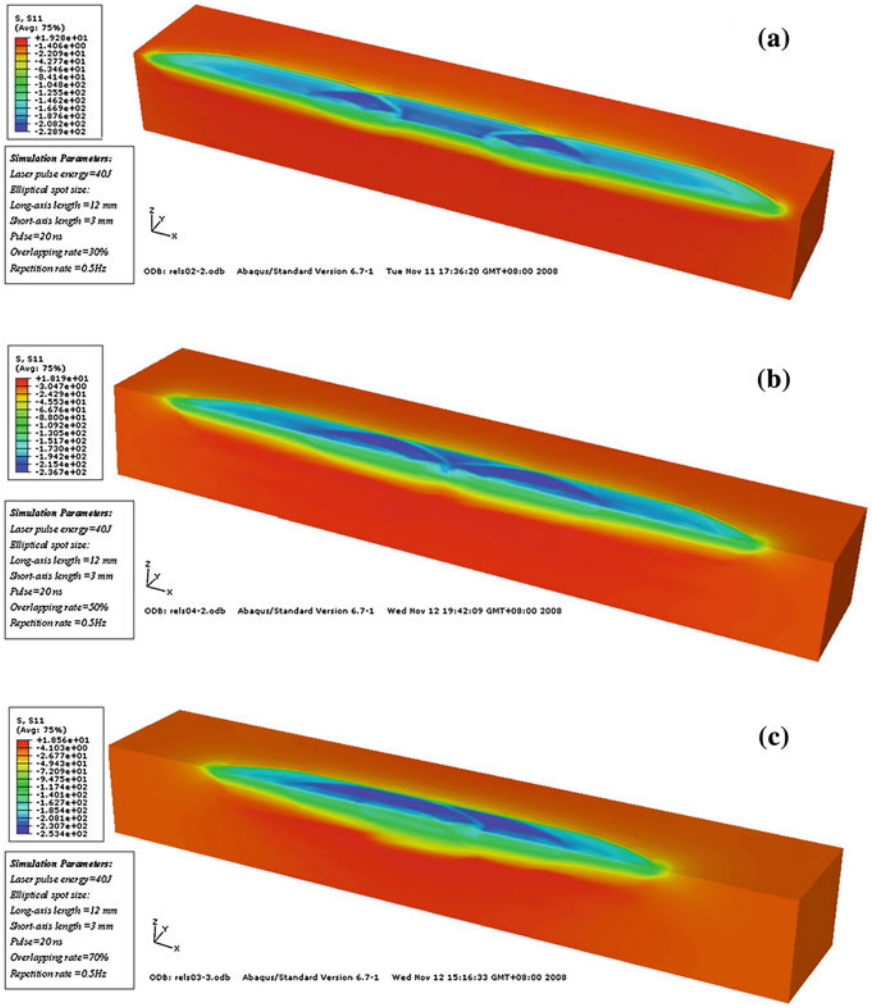

Fig. 2.24 Simulation model of residual stresses S11 by LSP with over lapping rates η_L **a** 30 %, **b** 50 %, **c** 70 %

two successive impacts on both sides. Obviously, it was about an increase of 33.7 % to −230 MPa for 30 and 50 % overlapping rate, and 47.1 % to −253 MPa for 70 % overlapping rate.

Under the 50 % overlapping rate, the fluctuation was about 4 %, and the good uniformity of surface residual stress along the symmetric plane was achieved. However, the fluctuation was increased by 23.5 % from −170 to −210 MPa for 30 % overlapping rate and by 15.4 % from −195 to −225 MPa for 70 % overlapping rate.

The results indicated that the fluctuation of LSP with 70 % overlapping rate was higher than that of LSP with 50 % overlapping rate due to the different

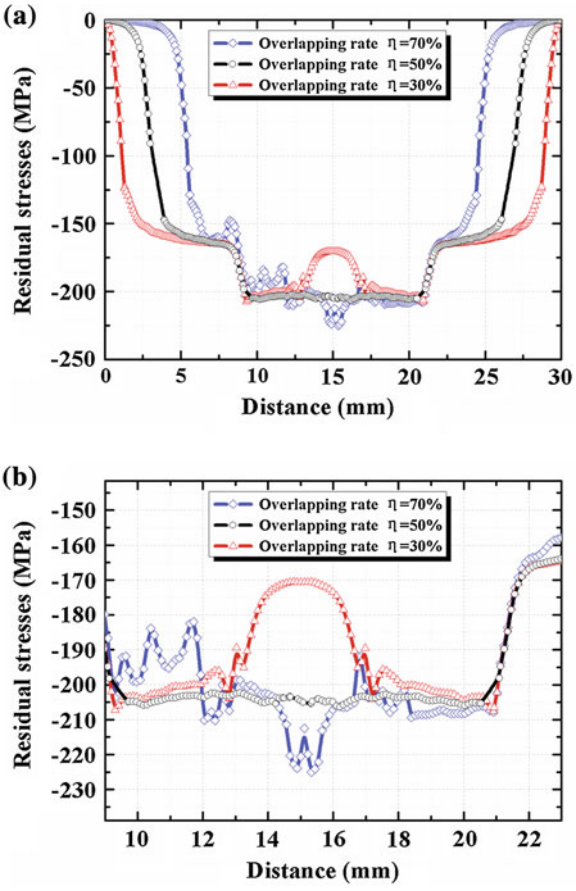

Fig. 2.25 FEM simulation of surface residual stress S11 by LSP with different overlapping rates. **a** Along X direction on *top* surface, **b** the enlarged partial view in over lapped regions

shocked number at various regions. The simulated data was nonsymmetrical along the symmetric plane due to different shocked order.

Figure 2.26 showed the distribution of surface residual stress measured on the top surface along the symmetric plane with different overlapping rates. The measured results were in good agreement with the simulated data. Figure 2.27 showed the schematic diagram of overlapping elliptical spots along the center line with different overlapping rates η_L (50, 70, and 80 %). From Fig. 2.27a, we can see that the regions along the symmetric plane were shocked two times while the overlapping rates η_L was 50 %, and the distribution of surface residual stresses at the regions was uniform. While the overlapping rates η_L is 70 %, it can be seen from Fig. 2.27b that the regions along the symmetric plane were shocked three times or four times, and the fluctuation of residual stress in the interesting region increased in comparison with that with the overlapping rate η_L 50 %. If the overlapping rates η_L is 80 %, it can be seen from Fig. 2.27c that the regions along the center line were shocked five times, and the homogeneity of surface residual

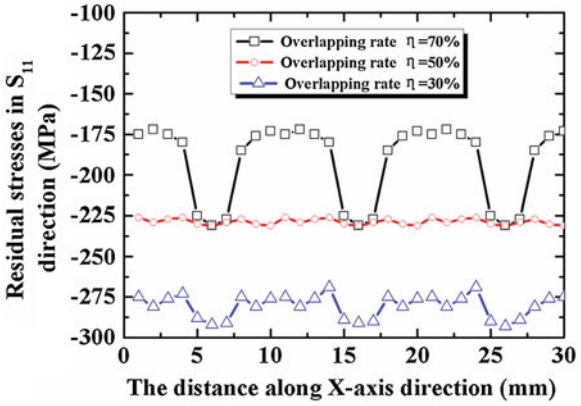

Fig. 2.26 The distribution of surface residual stress measured on the top surface along the symmetric plane with different over lapping rates

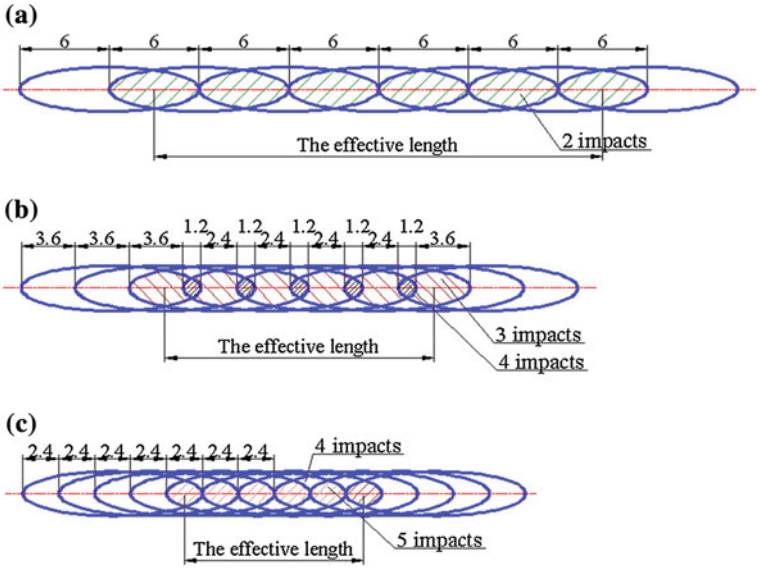

Fig. 2.27 The schematic diagram of over lapping elliptical spots along the symmetric plane with different over lapping rates η_L. **a** 50 %, **b** 70 %, **c** 80 %

stresses at the regions was good, but the magnitude of surface residual stresses remain unchanged in comparison with that with the overlapping rate η_L 50 %.

From the above studied results, we can make the following inferences. First, it is not the fact that the higher the overlapping rate is, the better the uniformity of the surface residual stress on the sample surface is. By compared to that with 50 % overlapping rate, the fluctuation of surface residual stress with 70 % overlapping rate is high. The higher the overlapping rate is and the more the shocked number

is, the higher the magnitude of surface residual stress is. However, when the shocked number exceeds four times, the surface residual stress is kept to be the constant because the plastic deformation near the surface is almost saturated [80]. Hence, the increase of overlapping rate can enhance the values of surface residual stresses in repetitive-impacted regions within a certain impact-number range of 1–4 times, but can't effectively make it more uniform. Second, the higher the overlapping rate is, the smaller the effective shocked-length is. From Fig. 2.27, we can see that the effective lengths with the overlapping rate of 50, 70 and 80 % are 30, 18 and 12 mm under the same shocked-number, respectively. The bigger effective shocked-length can be obtained by using the smaller overlapping rate during LSP, thus the efficiency of the LSP can be improved.

2.7.4 The Simulation and Verification of Residual Stress Distribution in Depth Direction

The simulated residual stresses were obtained from the surface element located at the center of the laser spot. A comparison of the simulated and measured residual stress values were shown in Fig. 2.28. Both the simulated and measured residual stresses were compressive, which are agreed with the trend.

Figure 2.29 showed the comparison of simulated residual stress S11 in depth direction with measured data. The simulated and measured in-depth residual stresses in the regions after 1 impact, 2 impacts and 3 impacts as functions of the distance from the surface were shown in Figs. 2.29a, b, respectively. It can be seen that the compressive residual stresses existed in the subsurface for both cases and the maximum magnitudes were located at the surface.

It is well known that the compressive residual stresses near the sample surface are generated due to the local plastic deformation after LSP. Both the simulated and measured residual stresses are on the whole consistent. When the distance from the surface is higher than the certain value (e.g., in the experiment it is about

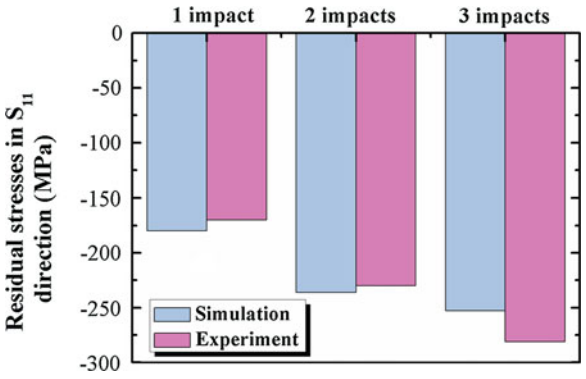

Fig. 2.28 Comparison of simulated surface residual stress S11 with measured data

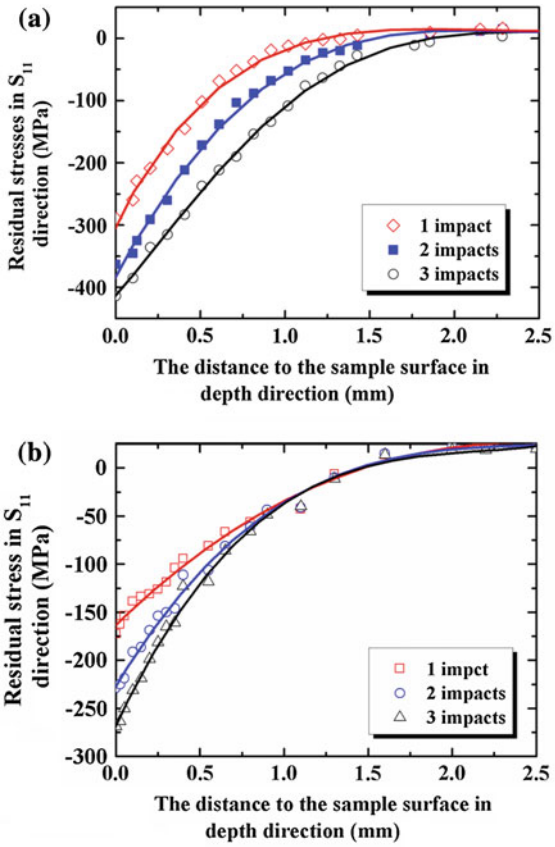

Fig. 2.29 Comparison of simulated in-depth residual stress S11 with measured data **a** simulated data, **b** measured data

1.5 mm and in the simulation is about 2.0 mm in the present work), the residual stresses in the subsurface are almost not sensitive to the number of the laser impacts. However, when the distance from the surface is lower than the certain value, the number of the laser impacts has an important influence on the change of residual stress in depth direction. Hence, in order to increase the residual stress near the surface, the number of the laser impacts should be increased, but increasing the shock number cannot enough effectively to increase the plastically affected depth.

Some discrepancy between simulation and experiment may be due to several factors that different experimental procedure from the simulation. (1) The exact location of residual stress measurement with regard to the laser shocked region can't be accurately controlled in the experiment. (2) The magnitudes of the residual stress in depth direction were measured by using electropolishing material removal method, where the measured values need to be revised.

To obtain a homogeneous residual stress field, the overlapping rate should be optimized for the treatment. Laser impacts with 50 % overlapping rate can be used

to obtain the surface residual stress field of good uniformity for LSP of LY2 Al alloy. In addition, in view of work efficiency, overlapping rate which is set to 50 % can be used to achieve longer effective shocked length. Hence, proper selection of overlapping rate is of great importance for the treatment of large area LSP, which can induce a better residual stress field in the sample to enhance the surface performance of the metal materials.

2.8 Summary

This chapter experimentally investigates and analyzes the effects of LSP on nano-hardness, elastic modulus and surface topography of the sample manufactured by LY2 Al alloy, and simulates and experimentally investigates the effects of overlapping rate on residual stress of LY2 Al alloy subjected to LSP with the elliptical spot. Some important conclusions can be summarized by the following statements:

(1) The values of nano-hardness and elastic modulus in the laser-shocked region and the laser-affected region were clearly larger than those in the non-shocked region. The contact depths in the laser-shocked region and the laser-affected region were lower than those in the non-shocked region, and the magnitude of nano-hardness in the laser-shocked region were greater from another point of view. The improvement of the elastic modulus and nano-hardness was favorable for improving FOD resistance of the components manufactured by LY2 Al alloy.
(2) The enhancement of LSP on nano-hardness and elastic modulus of LY2 Al alloy was mainly due to the grain refinement, the generation of high density dislocations and a small amount of twins.
(3) The initial surface topography plays a highly important role for LY2 Al alloy when treated by LSP. It will influence the surface topography, residual stress and micro-hardness.
(4) The surface roughness of LY2 Al alloy will tend to stable after one LSP impact. There is an ultimate value of about 0.58 μm for the surface roughness of LY2 Al alloy after multiple LSP impacts. The corresponding surface height distribution scatters from −2.5 to 2.5 μm.
(5) The increasing surface roughness will decrease the compressive residual stress when subjected to one LSP impact. When subjected to three LSP impacts, the surface residual stress of all the samples tends to be saturated and the saturated compressive residual stress is independent of surface roughness.
(6) LSP can improve micro-hardness of LY2 Al alloy. The increasing surface roughness will increase the micro-hardness after one LSP impact. However, the initial surface topography has no influence on the micro-hardness of LY2 after multiple LSP impacts.
(7) The single and multiple LSP FEM simulations have been developed and the simulated residual stresses in surface and depth direction agree well with the measured data in nature and trend.

(8) The largest stress magnitudes are located on the top surface of the LY2 Al sample, and the increase of the laser shocked-number can increase the magnitude of residual stress near the surface within a certain impact-number range of 1–4 times, but it is not effective to increase the affected depth.
(9) The overlapping rate should be optimized and selected carefully for large area LSP. An appropriate overlapping rate is beneficial to obtain a homogeneous residual stress field, and 50 % overlapping rate can be selected for the LSP treatment of the LY2 Al alloy due to the shocked effect and the work efficiency.

References

1. Fairand, B. P., Wilcox, B. A., Gallagher, W. J., & Williams, D. N. (1972). Laser shock induced microstructural and mechanical property changes in 7075 Al. *Journal of Applied Physics, 43*, 3893–3895.
2. Peyre, P., Fabbro, R., Merrien, P., & Lieurade, H. P. (1996). Laser shock processing of Al alloys. Application to high cycle fatigue behaviour. *Materials Science and Engineering A, 210*, 102–113.
3. Ballard, P., Fournier, J., Fabbro, R., & Frelat, J. (1991). Residual stresses induced by laser-shocks. *Journal de Physique IV, C3*, 487–494.
4. Devaux, D., Fabbro, R., & Virmont, J. (1991). Generation of shock waves by laser–matter interaction in confined geometries. *Journal De Physique IV, 1*(C7), 179–182.
5. Peyre, P., & Fabbro, R. (1995). Electromagnetic gauge study of laser-induced shock waves in aluminium alloys. *Journal De Physique III France, 5*, 1953–1964.
6. Peyre, P., & Fabbro, R. (1995). Laser shock processing: a review of the physics and applications. *Optical and Quantum Electronics, 27*, 1213–1219.
7. Peyre, P., Merrien, P., Lieurade, H. P., & Fabbro, R. (1995). Laser induced shock waves as surface treatment for 7075–T7351 aluminium alloy. *Surface Engineering, 11*, 47–52.
8. Berthe, L., Fabbro, R., Peyre, P., Tollier, L., & Bartnicki, E. (1997). Shock waves from a water-confined laser-generated plasma. *Journal of Applied Physics, 82*, 2826–2832.
9. Vaccari, J. A. (1992). Laser shocking extends fatigue life. In J. A. Vaccari (Ed.), *Laser Technology* (pp. 62–64) American Machinist.
10. Dane, C. B., Hackel. L. A., Daly. J., & Harrison, J. (1997). High laser power for peening of metals enabling production technology. Advanced aerospace materials and processes Conference' 98. Tysons Corner,Virginia, June 15–18: 1998.
11. Tenaglia, R. D., & Lahrman, D. F. (2009). Shock tactics. *Nature Photonics, 3*, 267–269.
12. Fairand, B. P., Clauer, A. H., Jung, R. G., & Wilcox, B. A. (1974). Quantitative assessment of laser-induced stress waves generated at confined surfaces. *Applied Physics Letters, 25*, 431–433.
13. O'Keefe, J. D., & Skeen, C. H. (1972). Laser-induced stress-wave and impulse augmentation. *Applied Physics Letters, 21*, 464–466.
14. Hoffman, C. G. (1974). Laser–target interactions. *Journal of Applied Physics, 45*, 2125–2128.
15. Yang, L. C. (1974). Stress waves generated in thin metallic films by a Q-switched ruby laser. *Journal of Applied Physics, 45*, 2601–2607.
16. Ling, P., & Wight, C. A. (1995). Laser-generated shock waves in thin films of energetic materials. *Journal of Applied Physics, 78*, 7022–7025.
17. Couturier, S., Resseduier, M., Hallouin, M., Romain, J. P., & Bauer, F. (1996). Shock profile induced by short laser pulses. *Journal of Applied Physics, 79*, 9338–9342.

18. White, R. M. (1963). Elastic wave generation by electron bombardment or electromagnetic wave absorption. *Journal of Applied Physics, 34*, 2123–2124.
19. Skeen, C. H., & York, C. M. (1968). Laser-Induced blow-off phenomenon. *Applied Physics Letters, 12*, 369–371.
20. Clauer, A. H., Holbrook, J. H., & Fairand, B. P. (1981). Effects of laser induced shock waves on metals. In M. A. Meyers & L. E. Murr (Eds.), *Shock waves and high-strain-rate phenomena in metals* (pp. 675–702). New York: Plenum Publishing Corporation.
21. Fabbro, R., Fournier, J., Ballard, P., Devaux, D., & Virmont, J. (1990). Physical study of laser-produced plasma in confined geometry. *Journal of Applied Physics, 68*, 775–784.
22. Fairand, B. P., Wilcox, B. A., Gallagher, W. J., & Williams, D. N. (1972). Laser shock-induced microstructural and mechanical property changes in 7075 Al. *Journal of Applied Physics, 43*, 3893–3896.
23. Montross, C. S., Florea, V., & Bolger, J. A. (1999). Laser-induced shock wave generation and shock wave enhancement in basalt. *International Journal of Rock Mechanics and Mining Sciences, 36*, 849–855.
24. Fairand, B. P., Clauer, A. H., & Wilcox, B. A. (1977). Pulsed laser induced deformation in an Fe-3 Wt Pct Si alloy. *Metallurgical Transactions A, 8*, 119–125.
25. Clauer, A. H. (1996). Laser shock peening for fatigue resistance. In J. K. Gregory, H. J. Rack & D. Eylon (Eds.) *Surface performance of titanium* (pp. 217–230) Warrendale (PA): TMS.
26. Luong, H., & Hill, M. R. (2008). The effects of laser peening on high-cycle fatigue in 7085–T7651 Al alloy. *Materials Science and Engineering A, 477*, 208–216.
27. Zhang, Y. K., Zhang, X. R., Wang, X. D., Zhang, S. Y., Gao, C. Y., Zhou, J. Z., et al. (2001). Elastic properties modification in Al alloy induced by laser-shock processing. *Materials Science and Engineering A, 297*, 138–143.
28. Rubio-González, C., Ocańa, J. L., Gomez-Rosas, G., Molpeceres, C., Paredes, M., Banderas, A., et al. (2004). Effect of laser shock processing on fatigue crack growth and fracture toughness of 6061–T6 Al alloy. *Materials Science and Engineering A, 386*, 291–295.
29. Yang, J. M., Her, Y. C., Han, N., & Clauer, A. (2001). Laser shock peening on fatigue behavior of 2024–T3 Al alloy with fastener holes and stop holes. *Materials Science and Engineering A, 298*, 296–299.
30. Zhang, H., Zhang, Y. K., & Yu, C. Y. (1999). Surface treatment of Al alloy by laser shock processing. *Surface Engineering, 15*, 454–456.
31. Fourier, J. (1990). Mechanical effects induced by shock waves generated by high-energy laser pulses. *Materials Manufacturing Processes, 5*, 144–147.
32. Sánchez-Santana, U., Rubio-González, C., Gomez-Rosas, G., Ocana, J. L., Porro, J., & Morales, M. (2006). Wear and friction of 6061–T6 Al alloy treated by laser shock processing. *Wear, 260*, 847–854.
33. Zhang, Y. K., Lu, J. Z., Ren, X. D., Yao, H. B., & Yao, H. X. (2009). Effect of laser shock processing on the mechanical properties and fatigue lives of the turbojet engine blades manufactured by LY2 Al alloy. *Materials and Design, 30*(5), 1697–1703.
34. Clauer, A. H., Fairand, B. P., & Wilcox, B. A. (1977). Laser shock hardening of weld zones in Al alloys. *Metallurgical and Materials Transactions A: Physical, 8*, 1871–1876.
35. Lu, J. Z., Zhang, L., Feng, A. X., Jiang, Y. F., & Cheng, G. G. (2009). Effects of laser shock processing on mechanical properties of Fe–Ni alloy. *Materials and Design, 30*(9), 3673–3678.
36. Read, D. T., & Dally, J. W. (1993). A new method for measuring the strength and ductility of thin films. *Journal of Materials Research, 8*(7), 1542–1549.
37. Weihs, T. P., Hong, S., Bravman, J. C., & Nix, W. D. (1998). Mechanical deflection of cantilever micro beams: A new technique for testing the mechanical properties of thin films. *Journal of Materials Research, 3*(5), 931–942.
38. Doerner, M. F., Gardner, D. S., & Nix, W. D. (1986). A method for interpreting the data from depth-sensing indentation instruments. *Journal of Materials Research, 1*(4), 601–609.

39. Wang, X. W., Wang, J. Y., Wu, P., & Zhang, H. W. (2004). The investigation of internal friction and elastic modulus in surface nanostructured materials. *Materials Science and Engineering A, 370*, 158–162.
40. San, J. F., Wang, Z. C., Li, S. H., & Liu, J. J. (2006). Nano-hardness and wear properties of C-implanted Nylon 6. *Surface and Coatings Technology, 200*(18–19), 5245–5252.
41. Bhatt, R. T., Choi, S. R., Cosgriff, L. M., Fox, D. S., & Lee, K. N. (2008). Impact resistance of uncoated SiC/SiC composites. *Materials Science and Engineering A, 476*, 20–28.
42. Chen, X., Wang, R., Yao, N., Evans, A. G., Hutchinson, J. W., & Bruce, R. W. (2003). Foreign object damage in a thermal barrier system: mechanisms and simulations. *Materials Science and Engineering A, 352*, 221–231.
43. Montross, C. S., Ye, L., Wei, T., Clark, G., & Mai, Y. W. (2002). Laser shock processing and its effects on microstructure and properties of metal alloys: a review. *International Journal of Fatigue, 24*, 1021–1036.
44. Montross, C. S., Brandt, M., & Swain, M. V. (2001). Self-limiting hardness changes in laser peened 6061–t6 aluminium. *Surface Engineering, 17*, 477–482.
45. Montross, C. S., Florea, V., Brandt, M., & Swain, M. V. (2000). Subsurface properties of laser peened 6061–T6 Al weldments. *Surface Engineering, 16*, 116–121.
46. Devaux, D., Fabbro, R., & Tollier, L. (1993). Generation of shock waves by laser-induced plasma in confined geometry. *Journal of Applied Physics, 74*, 2268–2273.
47. Chu, J. P., Rigsbee, J. M., Banas′, G., & Elsayed-Ali, H. E. (1999). Laser-shock processing effects on surface microstructure and mechanical properties of low carbon steel. *Materials Science and Engineering A, 260*, 260–268.
48. Ganin, E., Komem, Y., & Rosen, A. (1978). Shock induced hardness in α-Iron. *Materials Science and Engineering A, 33*, 1–4.
49. Yilbas, B. S., & Arif, A. F. M. (2007). Laser shock processing of Al: model and experimental study. *Journal of Physics. D. Applied Physics, 40*, 6740–6747.
50. McEvily, A. J., Renauld, M., & Bao, H. (1997). Fatigue fracture-surface roughness and the K-opening level. *International Journal of Fatigue, 19*, 629–633.
51. Romeiro, F., Freitas, M., & Fonte, M. (2009). Fatigue crack growth with overloads/under loads: Interaction effects and surface roughness. *International Journal of Fatigue, 31*, 1889–1894.
52. Zhang, Y. K., Zhang, S. Y., & Zhang, X. R. (1997). Laser ultrasound velocity of material with a surface coating layer. *Surface and Coatings Technology, 92*, 104–109.
53. Rozmus-Górnikowska, M. (2010). Surface modifications of a Ti6Al4 V alloy by a laser shock processing. *Acta Physica Polonica A, 117*, 808–811.
54. Luong, H., & Hill, M. R. (2008). The effects of laser peening on high-cycle fatigue in 7085–T7651 Al alloy. *Materials Science and Engineering A, 477*, 208–216.
55. WYKO Vision Software Help Document.
56. Rozmus-Górnikowska, M. (2010). Surface modifications of a Ti6Al4 V alloy by a laser shock processing. *Acta Physica Polonica A, 5*, 117–120.
57. Berthe, L., Fabbro, R., Peyre, P., Tollier, L., & Bartnicki, E. (1997). Shock waves from a water-confined laser-generated plasma. *Journal of Applied Physics, 82*, 2826–2832.
58. Guo, Y. B., & Caslaru, R. (2011). Fabrication and characterization of micro dent arrays produced by laser shock peening on titanium Ti–6Al–4 V surfaces. *Journal of Materials Processing Technology, 211*, 729–736.
59. Clauer, A. H., Holbrook J. H., Fairand. B. P. (1981). In M. A. Meyers & L. E. Murr (Eds.). Sh*ock waves and high-strain-rate phenomena in metals* (pp. 675–702). New York: Plenum Publishing Corporation.
60. Yilbas, B. S., & Arif, A. F. (2007). Laser shock processing of Al: model and experimental study. *Journal of Physics D Applied Physics, 40*, 6740–6747.
61. Zhang, Y. K., Hu, C. L., Cai, L., Yang, J. C., & Zhang, X. R. (2001). Mechanism of improvement on fatigue life of metal by laser-excited shock waves. *Applied Physics A, 72*(2), 113–116.

62. Yang, C. H., Hodgson, P. D., & Liu, Q. C. (2008). Geometrical effects on residual stresses in 7050–T7451 Al alloy rods subject to laser shock peening. *Journal of Materials Processing Technology, 201*, 303–309.
63. Rubio-González, C., Ocaña, J. L., & Gomez-Rosas, G. (2004). Effect of laser shock processing on fatigue crack growth and fracture toughness of 6061–T6 Al alloy. *Materials Science and Engineering A, 386*, 291–295.
64. Zhang, Y. K., Gu, Y. Y., Zhang, X. Q., & Zhou, J. (2006). Study of mechanism of overlay acting on laser shock waves. *Journal of Applied Physics, 100*, 103517-1.
65. Marchi, C. S., Zaleski, T., Lee, S., Yang, N. Y., & Stuart, B. (2008). Effect of laser peening on the hydrogen compatibility of corrosion-resistant nickel alloy. *Scripta Materials, 58*(9), 782–785.
66. Zhang, Y. K., Zhang, S. Y., & Cai, L. (1997). Investigation of surface qualities of laser shock-processes zones and the effect on the fatigue life of Al alloy. *Surface and Coatings Technology, 92*, 104–107.
67. Warren, A. W., Guo, Y. B., & Chen, S. C. (2008). Massive parallel laser shock peening: Simulation, analysis, and validation. *International Journal of Fatigue, 30*(1), 188–197.
68. Dane, C. B., Hackel, L. A., Daly, J., & Harrisson, J. (1997). Laser peening of metals-enabling laser technology. *Advanced Materials Processes, 5*, 13–27.
69. Vaccari, J. A. (1992). Laser shocking extends fatigue life. *American Machine, 6*, 62–64.
70. Ding, K., & Ye, L. (2003). Three-dimensional dynamic finite element analysis of multiple laser shock peening processes. *Surface Engineering, 19*, 351–358.
71. Hu, Y. X., Yao, Z. Q., & Hu, J. (2006). 3-D FEM simulation of laser shock processing. *Surface and Coatings Technology, 201*, 1426–1435.
72. Nalla, R. K., Altenberger, I., Noster, U., Liu, G. Y., Scholtes, B., & Ritchie, R. O. (2003). On the influence of mechanical surface treatments-deep rolling and laser shock peening-on the fatigue behavior of Ti-6Al-4 V at ambient and elevated temperatures. *Materials Science and Engineering A, 355*, 216–230.
73. Nikitin, I., Sholtes, B., Maier, H. J., & Altenberger, I. (2004). High temperature fatigue behavior and residual stress stability of laser-shock peened and deep rolled. *Scripta Materials, 50*(10), 1345–1350.
74. Hu, Y. X., & Yao, Z. Q. (2008). FEM simulation of residual stresses induced by laser shock with overlapping laser spots. *Acta Metallurgica Sinica (English Letters), 21*(2), 125–132.
75. Evans, A. D., Bruno, G., King, A., Withers, P. J. (2002). Laser shock peening for aerospace Ti-6Al-4 V alloy: a residual stress study. Annual report of the institut Laue-Langevin (ILL), pp. 42–43.
76. Clauer, H. A., Walters, C. T., & Ford, S. C. (1983). The effects of laser shock processing on the fatigue properties of -T3 Al. In *Lasers in materials processing.* Metals Park (OH), American Society for Metals, pp 7–22.
77. ABAQUS, Inc. (2012). ABAQUS User's Manual, Ver. 6.12, Pawtucket, RI.
78. Ding, K., & Ye, L. (2003). FEM simulation of two sided laser shock peening of thin sections of Ti-6Al-4 V alloy. *Surface Engineering, 19*, 127–133.
79. Yakimets, I., Richard, C., Beranger, G., & Peyre, P. (2004). Laser peening processing effect on mechanical and tribological properties of rolling steel 100Cr6. *Wear, 256*(3–4), 311–320.
80. Evans A. D., Bruno G., King A., & Withers P. J. (2002) Laser shock peening for aerospace Ti–6Al–4 V alloy: a residual stress study. Annual Report of the Institut Laue-Langevin (ILL), Grenoble, France, pp. 42–43.

http://www.springer.com/978-3-642-35673-5

Laser Shock Processing of FCC Metals
Mechanical Properties and Micro-structural
Strengthening Mechanism

Zhang, Y.; Lu, J.; Luo, K.

2013, XI, 194 p., Hardcover
ISBN: 978-3-642-35673-5